Mon. Not. R. Astron. Soc. **376,** 157–172 (2007) doi:10.1111/j.1365-2966.2006.11369.x

The strong transformation of spiral galaxies infalling into massive clusters at $z \approx 0.2$

L. Cortese,[1⋆] D. Marcillac,[2] J. Richard,[3] H. Bravo-Alfaro,[4] J.-P. Kneib,[5] G. Rieke,[2] G. Covone,[6] E. Egami,[2] J. Rigby,[2] O. Czoske[7] and J. Davies[1]

[1]*School of Physics and Astronomy, Cardiff University, Cardiff CF24 3AA*
[2]*Steward Observatory, University of Arizona, 933 N. Cherry Avenue, Tucson, AZ 85721, USA*
[3]*Caltech, Astronomy 105-24, Pasadena, CA 91125, USA*
[4]*Departamento de Astronomia, Universidad de Guanajuato, Apdo. Postal 144, 36000 Guanajuato, Mexico*
[5]*Laboratoire d'Astrophysique de Marseille, Traverse du Siphon, BP8 13376 Marseille, France*
[6]*INAF-Osservatorio Astronomico di Capodimonte, 80131 Napoli, Italy*
[7]*Argelander-Institut für Astronomie, Universität Bonn, Auf dem Hügel 71, 53121 Bonn, Germany*

Accepted 2006 December 1. Received 2006 November 30; in original form 2006 August 10

ABSTRACT

We describe two peculiar galaxies falling into the massive galaxy clusters Abell 1689 ($z \approx 0.18$) and Abell 2667 ($z \approx 0.23$), respectively. *Hubble Space Telescope* (*HST*) images show extraordinary trails composed of bright blue knots ($-16.5 < M < -11.5$ mag) and stellar streams associated with each of these systems. Combining optical, near- and mid-infrared and radio observations we prove that while both galaxies show similar extended trails of star-forming knots, their recent star formation histories are different. One ($\approx L^*$) is experiencing a strong burst of star formation, appearing as a rare example of a luminous infrared cluster galaxy. In comparison, the other ($\approx 0.1L^*$) has recently ceased its star formation activity. Our model suggests that the morphologies and star formation in these galaxies have been influenced by the combined action of tidal interaction (likely with the cluster potential) and of ram pressure with the intracluster medium (ICM). These results can be used to gain more insights to the origin of S0s, dwarf and ultracompact dwarf (UCD) cluster galaxies.

Key words: galaxies: clusters: individual: A1689 – galaxies: clusters: individual: A2667 – galaxies: evolution – galaxies: high-redshift – galaxies: interactions – galaxies: peculiar.

1 INTRODUCTION

Clusters are natural laboratories to study the effects of environment on the evolution of galaxies (Dressler 1980). A plethora of evidence shows that the properties of late-type galaxies depend strongly on environment: besides the well-known morphology–density relation (Dressler 1980; Whitmore, Gilmore & Jones 1993), in local clusters ($z \leqslant 0.03$) spiral galaxies are deficient in neutral hydrogen (Giovanelli & Haynes 1985; Cayatte et al. 1990; Bravo-Alfaro et al. 2000) and have lower star formation activity than galaxies of similar type and size in low-density environments (Lewis et al. 2002; Gómez et al. 2003; Gavazzi et al. 2006). Various physical mechanisms have been proposed to explain the different evolution of late-type spirals in clusters and in the field. In general, they invoke either dynamical interactions of cluster galaxies with the hot intracluster medium (ICM; Gunn & Gott 1972; Larson, Tinsley & Caldwell 1980) or gravitational interactions with nearby companions (Merritt 1983), with the potential of the cluster (Byrd & Valtonen 1990; Valluri 1993), or with a combination of these two (Moore et al. 1996). Interactions with the ICM are likely to be the dominant process at the present epoch and can account for the truncation of the gas discs in members of several local clusters (see Boselli & Gavazzi 2006 and references therein). However, ram pressure cannot produce the strong morphology–density relation (Dressler 1980; Whitmore et al. 1993), nor can it thicken the disc of a spiral galaxy and transform it into an S0 (i.e. Hinz, Rieke & Caldwell 2003; Christlein & Zabludoff 2004; Boselli et al. 2006).

This apparent contradiction could be solved if the structures form hierarchically; that is, if galaxy clusters form not by accreting individual galaxies randomly from the field, but rather by the infall of less massive groups along filaments. These infalling groups have velocity dispersions that are much smaller than that of the cluster as a whole, permitting the slow, strong interactions normally associated with field galaxies (Dressler 2004; Fujita 2004; Mihos 2004; Cortese et al. 2006b). Therefore, a plausible evolutionary history would take into account that environmental conditions and the physical properties of galaxies are changed significantly during cosmic

⋆E-mail: luca.cortese@astro.cf.ac.uk

time, changing the influence of various physical mechanisms on the evolution of galaxies (Boselli & Gavazzi 2006). However, this hypothesis is far from confirmed, since we lack detailed understanding of the range of environmental effects that act as a function of the age of the Universe (Dressler 2004). Although star-forming galaxies in clusters at intermediate redshift appear more disturbed (Oemler, Dressler & Butcher 1997; Couch et al. 1998) and have higher star formation activity (Butcher & Oemler 1978, 1984; Fadda et al. 2000) than local disc galaxies, it is still an open question which mechanisms are at play and how they influence the evolutionary history of cluster galaxies (Balogh et al. 1999; Dressler et al. 1999; Treu et al. 2003). To solve this riddle, we need to observe galaxies that physical circumstances and chance have revealed in rare moments of transformation. These peculiar systems can be used to probe different environmental effects and to constrain models of the evolutionary history of galaxies. Much of our knowledge on the evolution of nearby galaxies in both groups (Duc et al. 2000; Iglesias-Páramo & Vílchez 2001; Sulentic et al. 2001) and clusters (Kenney et al. 1995; Gavazzi et al. 2001; Vollmer et al. 2001, 2004; Boselli et al. 2005; Cortese et al. 2006b) has in fact come from studying of such systems. Unfortunately this information is difficult to extend to high redshift because both clusters and galaxies have evolved significantly: clusters were less relaxed (Jeltema et al. 2005) and galaxies had higher gas content. Therefore, the effects of the same environmental mechanisms could depend strongly on the age of the Universe.

In this paper, we present a multiwavelength analysis of two peculiar galaxies (hereafter referred as 235144−260358 and 131124−012040) falling into the centres of the massive clusters Abell 2667 ($z \approx 0.23$) and Abell 1689 ($z \approx 0.18$). Both these systems are associated with extended trails of bright blue knots and diffuse wisps and filaments of young stars, features observed so far only in one other galaxy at similar redshift (Owen et al. 2006). These two objects have been serendipitously detected by looking at the Wide Field Planetary Camera 2 (WFPC2) and Advanced Camera for Survey (ACS) images of massive clusters at $z \approx 0.2$. The sample of clusters consists of the 10 clusters discussed in Smith et al. (2005) plus A2667, A2390 and A1689. We therefore found two galaxies with extended trails within 13 studied clusters all located at $0.175 < z < 0.25$, suggesting that we are observing a very short snapshot of a critical stage in the evolution of these cluster galaxies.

Because these two systems have significantly different optical luminosities ($\approx L^*$ and $\approx 0.1L^*$) but are at similar distances from the cores of clusters of similar mass, they represent an interesting case for a comparison of the effects of similar environments on different-sized galaxies. Throughout this paper we assume a cosmology with $\Omega_{\rm m} = 0.3$, $\Omega_\lambda = 0.7$ and $H_0 = 70\,{\rm km\,s^{-1}\,Mpc^{-1}}$, implying a distance modulus of 39.74 (40.33) mag and a linear scale of 3.16 (3.71) kpc arcsec^{-1} for A1689 (A2667).

2 THE DATA

2.1 Optical photometry

The optical photometric data for this paper (Figs 1–3) are extracted from deep *Hubble Space Telescope* (*HST*) images of Abell 2667 and 1689. Abell 2667 was observed on 2001 October, using the WFPC2 for total exposures of 1200 s through the F450W filter, and 4000 s in F606W and F814W (see Figs 1 and 3) (Covone et al. 2006a). The 3σ detection limit for point sources is ≈26.00, 26.00 and 25.00 mag in the F450W, F606W and F814W bands, respectively. Deep observations of Abell 1689 were obtained from the ACS Guaranteed Time Observations in 2002 June (see Figs 2 and 3). A total of 20 orbits (≈13.2 h) were taken in the three pass bands F475W, F625W and F850LP (Broadhurst et al. 2005). The 3σ detection limit for point sources is ≈29.70, 29.20 and 28.30 mag in the filters F475W, F625W and F850LP, respectively.

We used SExtractor (Bertin & Arnouts 1996) to detect and analyse the sources. For source detection, we used an image averaging the three band passes; magnitudes were then determined from aperture photometry on the separate images for each filter. All magnitudes are in the VEGAMAG systems. No correction for Galactic extinction was performed ($A_V \leqslant 0.07$ mag). Surface brightness profiles for these galaxies were computed using the task ELLIPSE within IRAF. The ellipticity and position angle were determined using the *I*-band images following the procedure of Gavazzi et al. (2000). The disturbed morphologies of 235144−260358 in A2667 could possibly affect the shape of the surface brightness profiles at large radii (in particular at shorter wavelengths), but not in the central regions where both the objects still present a reasonably symmetrical shape. This is not the case of the edge-on spiral 131124−012040 which does not show strong asymmetries within the optical radius.

2.2 Near-infrared photometry

Near-infrared *H*-band observations for Abell 2667 and 1689 were obtained with the Infrared Spectrometer And Array Camera (ISAAC) on the Very Large Telescope (VLT) in the spring of 2003 [ESO (European Southern Observatory) Programs 071.A-0428, PI Kneib and 067.A-0095, PI Knudsen], under photometric sky conditions with a mean seeing of ≈0.41 and ≈0.58 arcsec, respectively. The total exposure time of 6529 s for each cluster corresponds to a 5σ detection limit for point sources of ≈24.6 mag. All these observations have been reduced as described in Richard et al. (2006).

2.3 Mid-infrared photometry

Spitzer imaging observations of Abell 2667 and 1689 were obtained as part of the GTO Lensing Cluster Survey (Program 83, PI Rieke). Multiband Imaging Photometry for Spitzer (MIPS) (Rieke et al. 2004) 24-μm images were obtained in photometry mode, with a total exposure time of ≈2700 s. The data were processed and mosaicked following the procedures described in Egami et al. (2006). Point-source extraction and photometry were performed using DAOPHOT (Stetson 1987) as described in Papovich et al. (2004). A point spread function (PSF) was constructed from the best-measured 30 point sources in the field; the Tiny Tim model of the 24-μm PSF (Krist 1995) was used to compute the aperture correction. 131124−012040 in Abell 1689 is not detected in MIPS images. We derived a 3σ limit using a photometry aperture radius of 6 arcsec, a sky annulus between 6 and 13 arcsec and an aperture correction of 1.698.

Infrared Array Camera (IRAC) (Fazio et al. 2004) four-bands (3.6, 4.5, 5.8 and 8.0 μm) imaging was also obtained, with a total exposure time of 2400 s band^{-1} for each cluster. Basic calibrated data were combined using a custom IDL mosaicking routine. For A2667 photometry was performed within apertures of radius ≈8.3 arcsec and no aperture corrections were applied because they are small with this large an extraction aperture. In contrast, in A1689 photometry was performed within a smaller aperture to avoid light contamination from nearby sources. We adopted a radius ≈2.4 arcsec, sky annulus between 2.4 and 7.2 arcsec and aperture corrections of 1.213, 1.234, 1.379 and 1.584 at 3.6, 4.5, 5.8 and 8.0 μm, respectively.

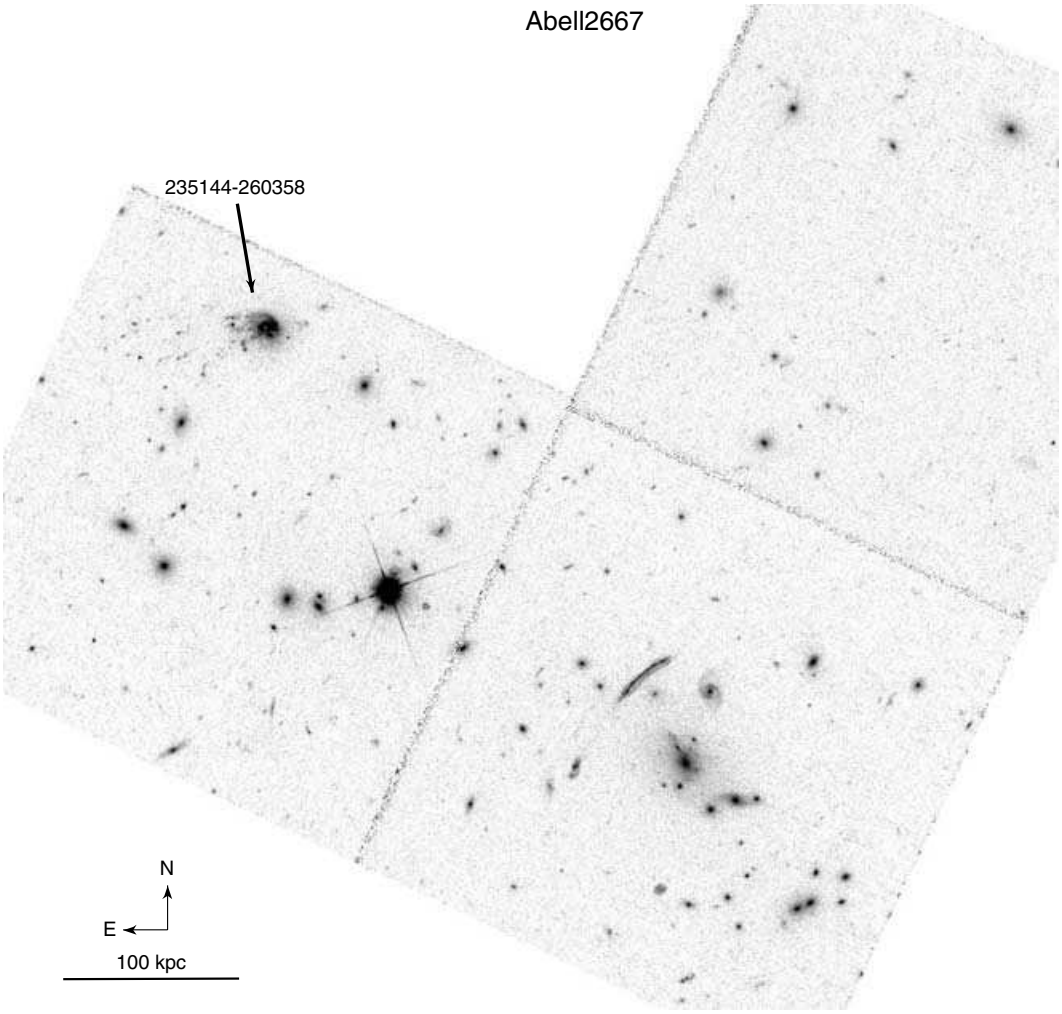

Figure 1. *HST*-WFPC2 F450W image of Abell 2667. The position of 235144−260358 is indicated.

2.4 Radio continuum observations

We obtained a 20-cm radio continuum measurement of ≈1.4 mJy for the galaxy in A2667 from the 1.4-GHz NRAO VLA Sky Survey (NVSS) continuum survey. As this survey offers rather poor spatial resolution (≈45 arcsec), we also constructed a 20-cm map using higher resolution data from the National Radio Astronomy Observatories (NRAO) Very Large Array (VLA) data archive. Two different observations are available on A2667 at this frequency: (1) it was observed in 2001 October for 3590 s in correlator mode 4, with a bandwidth of 25 MHz, and using the CD configuration (due to the low declination) and (2) a 3620-s observation was obtained in 2002 September with the same correlator mode and bandwidth, but in the BC configuration. We applied standard VLA calibration and imaging procedures with the Astronomical Image Processing System (AIPS). We then combined the two data sets in the *UV* plane using DBCON. Images were generated with the task IMAGR and a weighting option *robust* = 0, producing a map intermediate between natural and uniform weighting. After CLEANing, the resulting continuum map has a beam size of 16.7 × 13.1 arcsec^2 and an average rms noise of 0.12 mJy beam^{-1}.

The cluster A1689 was observed with the VLA for a total of 17 405 s in the A configuration in 2000 November and 2002 March. Combining the data sets using natural weighting (to improve the sensitivity) we produced a map with a beam size of 2.1 × 1.6 arcsec^2 and an average rms of 0.15 mJy beam^{-1}. No emission is detected at the position of the infalling galaxy. Taking a conservative detection threshold of 6σ we estimate an upper limit of 0.90 mJy for the 20-cm radio continuum flux.

2.5 Optical spectroscopy

We obtained optical spectroscopy for 131124−012040 in Abell 1689 as part of a wide field (≈30 × 30 arcsec^2) spectroscopic survey of the whole cluster (Czoske 2004; Czoske et al., in preparation) using Visible Multi-Object Spectrograph (VIMOS) on the VLT (Program 71.A-3065, PI Czoske). The LR-Blue grism was used, which provided a resolution of $R \approx 200$ over a wavelength range from 3750 to 6750 Å. The dispersion was 5.35 Å pixel^{-1}. We obtained three exposures of 840 s for a total of 42 min. The data were reduced using VIMOS Interactive Pipeline Graphical Interface (VIPGI) (Scodeggio et al. 2005) on site at IASF in Milano. The reduction involved bias subtraction, identification of the spectrum on the two-dimensional (2D) spectral image, interactive wavelength calibration from observations of arc spectra and optimal extraction using the method of Horne (1986). The spectrum has been flux

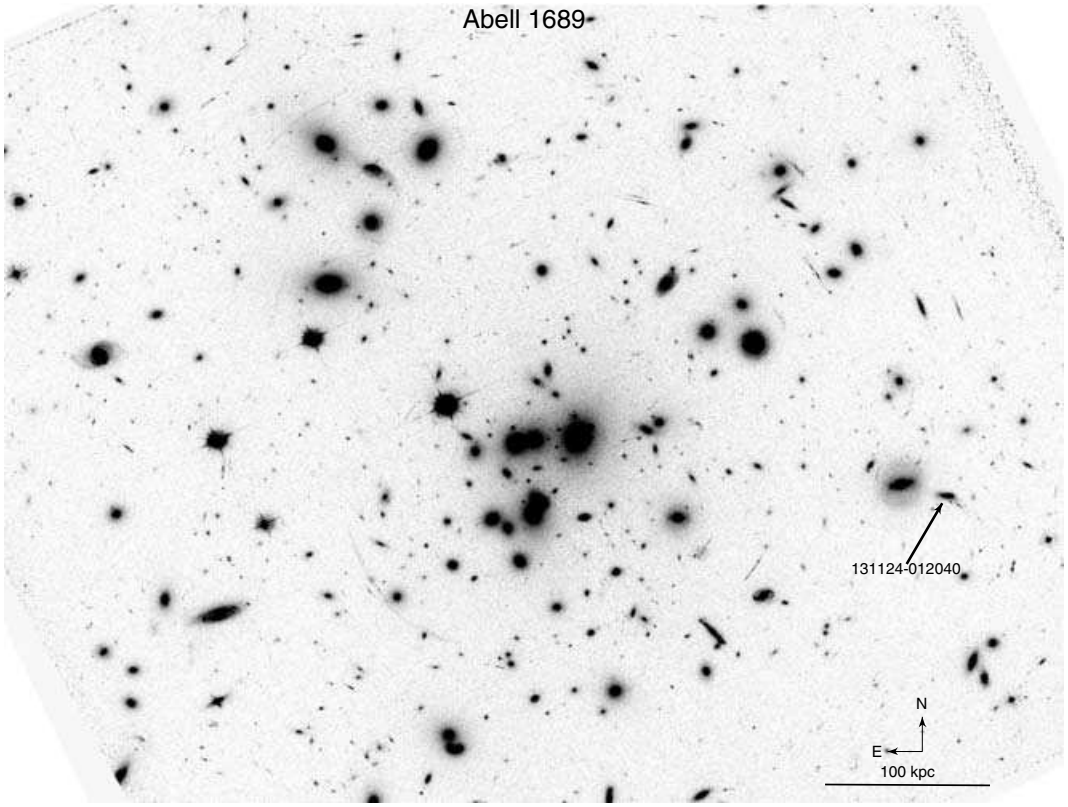

Figure 2. *HST*-ACS F475W image of Abell 1689. The position of 131124−012040 is indicated.

calibrated from observations of a spectrophotometric standard star, Feige 110.

In addition, we observed A2667 and A1689 in 2006 June with the Low Resolution Imaging Spectrograph (LRIS) instrument (Oke et al. 1995) on Keck I. A 5600-Å dichroic separated the red channel of the instrument, equipped with a 400 l mm^{-1} grating blazed at 8500 Å, from the blue channel, equipped with a 600 l mm^{-1} grism blazed at 4000 Å. This setting covers the wavelength range 3300–9200 Å with a dispersion of 0.6/1.8 Å and a resolution of 4.3/6.3 Å in the blue/red channel, respectively. On June 29, a 175-arcsec-long and 1-arcsec-wide slit was aligned on the centre of 235144−260358 in A2667 including two of its knots (K1 and K2), using a position angle of 92.7 east of north. Two exposures of 900 s were obtained under ≈1.5-arcsec seeing. On June 30, a 30-slits mask was used on A1689 in order to target multiple-imaged candidates at the cluster centre. One blue knot associated with the disrupted galaxy was included in a 9-arcsec-long and 1-arcsec-wide slit from this mask. Four exposures of 1800 s each have been obtained with an average seeing of 1.0 arcsec. All these spectroscopic data were reduced using standard IRAF procedures for flat fielding, wavelength and flux calibrations, sky subtraction and extraction of the spectra.

Under visual inspection of the spectra we carried out the measurement of the emission and absorption lines using the task SPLOT in IRAF. For the spectrum of 235144−260358 in Abell 2667 we de-blended the underlying absorption from the Hβ emission lines as discussed in Gavazzi et al. (2004). We evaluated the Balmer decrement from the ratio Hβ/Hα (assuming $T = 10\,000$ K and $n = 100$ e cm^{-3}; Osterbrock 1989) and derived the corrected line fluxes, relative to Hβ, using the dereddening law of Lequeux et al. (1979). The observed Hα/Hβ ratio for 235144−260358 is ≈3.65 implying a gas attenuation $A(\mathrm{H}\,\alpha) \approx 0.56$ mag and a stellar continuum attenuation $A(V) \approx 0.31$ mag (assuming the Galactic extinction curve; Pei 1992).

2.6 X-ray imaging

We downloaded the 9.2-ks *Chandra* ACIS (AXAF CCD Imaging Spectrometer) observation of A2667 from the public archive and reduced it following the standard 'threads' from CIAO data analysis software (version 3.3).[1] We searched the exposure-corrected images for sources, using the task WAVDETECT with angular wavelet scales from Brandt et al. (2001) and a significance threshold of 1×10^{-7}. No source is detected at the position of 235144−260358. We measure an upper limit to the 2–8 keV flux of 1.2×10^{-14} erg s^{-1} cm^{-2}.

3 RESULTS

3.1 Abell 2667

Fig. 3 (upper panel) shows an RGB image of 235144−260358 in Abell 2667, and its global properties are summarized in Table 1. Its optical redshift is $z \approx 0.2265$, lying in the low velocity tail of the velocity distribution of Abell 2667 (i.e. ≈830 km s^{-1} lower than the mean cluster velocity; Covone et al. 2006a). This face-on galaxy lies at a projected distance of $\approx 0.34\,h_{70}^{-1}$ Mpc from the cluster centre (assumed to coincide with the position of the central cD galaxy of A2667, see Fig. 1). This system is one of the brightest galaxies in the cluster (Covone et al. 2006a),

[1] http://cxc.harvard.edu/ciao/index.html

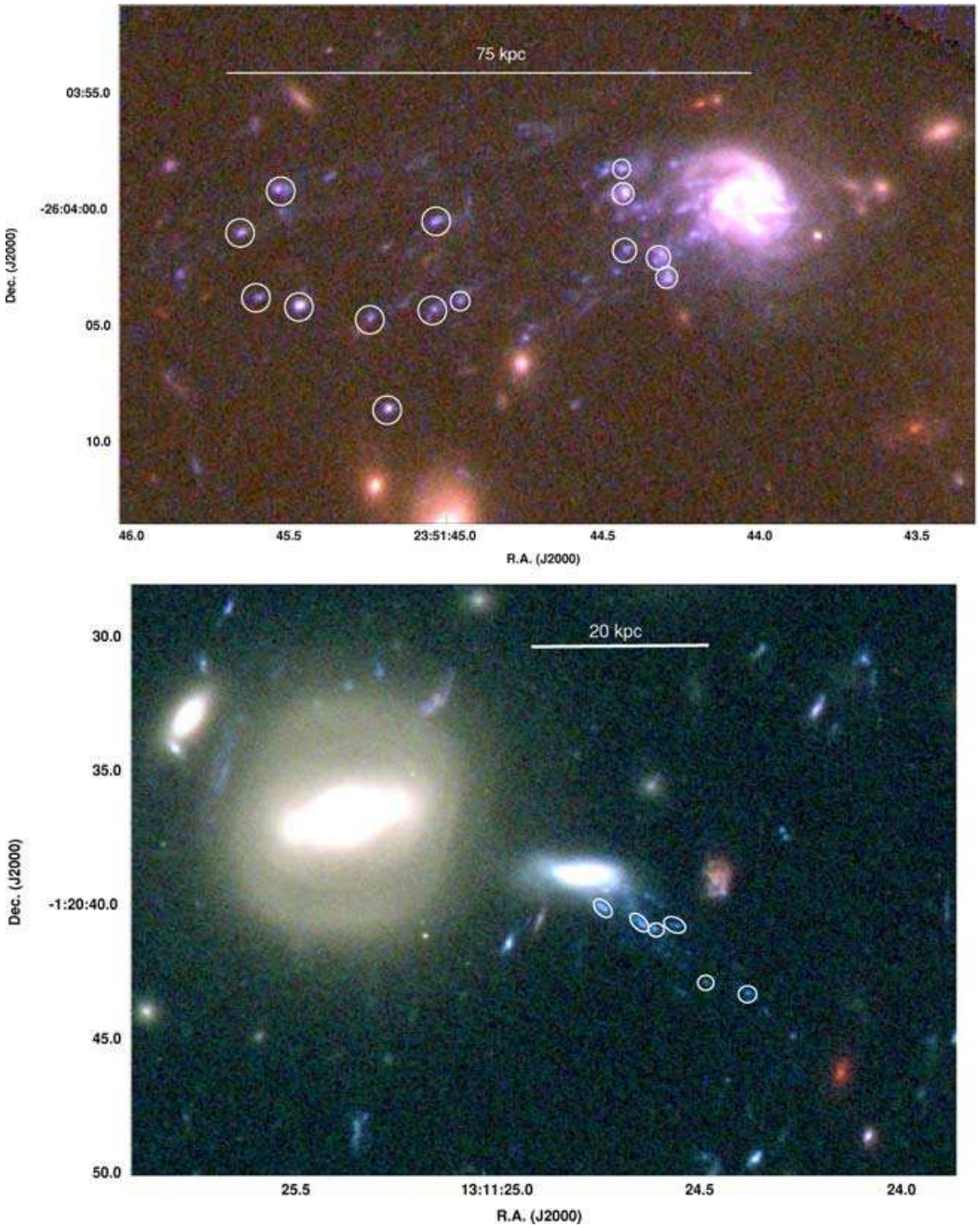

Figure 3. RGB colour image of 235144−260358 in Abell 2667 (upper panel) and of 131124−012040 in Abell 1689 (lower panel). The white circles indicate the knots studied in Section 3. This figure is in colour in the online version of the article on *Synergy*.

with both optical and near-infrared ($M_{F450W} \approx -21.50$, $M_H \approx -24.50$) absolute magnitudes close to L^* and a gas metallicity[2] of $12 + \log(O/H) \approx 9.0 \pm 0.1$ (i.e. ≈1.4 solar metallicity, see Fig. 7). From the *HST* images, 235144−260358 appears to be a late-type galaxy (see Fig. 3), as confirmed by its structural parameters (see Table 1). However, this object is definitely not normal: it shows a disturbed morphology, with clear indications of stripping within its optical disc and a prominent one-armed spiral component as is typically observed in gravitationally perturbed systems (Vollmer 2003). Moreover, there is a significant nuclear enhancement in the optical surface brightness profiles (≈2 mag within the central kpc; see Fig. 4), suggesting that it is experiencing a nuclear burst of star formation. This spike is particularly evident in the F450W band, where the central regions cannot be fitted with a simple deVaucouleurs profile.

Spitzer observations of A2667 expand on the unusual properties of 235144−260358, since it is detected by both IRAC (3.6–8 μm, see also Fig. 5) and MIPS (24 μm). At $z \approx 0.23$, the 8-μm emission

[2] The gas metallicity has been computed from the average of five different empirical determinations based on the following: R_{23} (McGaugh 1991; Zaritsky, Kennicutt & Huchra 1994); [N II] λ6583/[O II] λ3727 (Kewley & Dopita 2002); [N II] λ6583/H α (van Zee et al. 1998) and [O III] λ5007/[N II] λ6583 (Dutil & Roy 1999).

Table 1. Properties of the two disrupted galaxies.

	A1689 131124−012040		A2667 235144−260358
α (J2000)	13:11:24.86	α (J2000)	23:51:44.03
δ (J2000)	−01:20:39.9	δ (J2000	−26:03:59.6
z	0.1870	z	0.2265
F475W (mag)	−19.09	F450W (mag)	−21.54
F625W (mag)	−19.95	F606W (mag)	−22.20
F850LP (mag)	−20.49	F814W (mag)	−22.87
H (mag)	−21.82	H (mag)	−24.47
F(3.6 μm) (mJy)	0.026	F(3.6 μm) (mJy)	0.41
F(4.5 μm) (mJy)	0.019	F(4.5 μm) (mJy)	0.43
F(5.8 μm) (mJy)	0.005	F(5.8 μm) (mJy)	0.29
F(8 μm) (mJy)	0.008	F(8 μm) (mJy)	1.81
F(24 μm) (mJy)	<0.03	F(24 μm) (mJy)	4.20
F(20 cm) (mJy)	<0.90	F(20 cm) (mJy)	1.40
r_e (F850LP) (h_{70}^{-1} kpc)	3.1	r_e (F814W) (h_{70}^{-1} kpc)	5.5
μ_e (F850LP) (mag arcsec^{-2})	20.07	μ_e (F814W) (mag arcsec^{-2})	19.99
C_{31} (F850LP)	3.13	C_{31} (F814W)	3.02

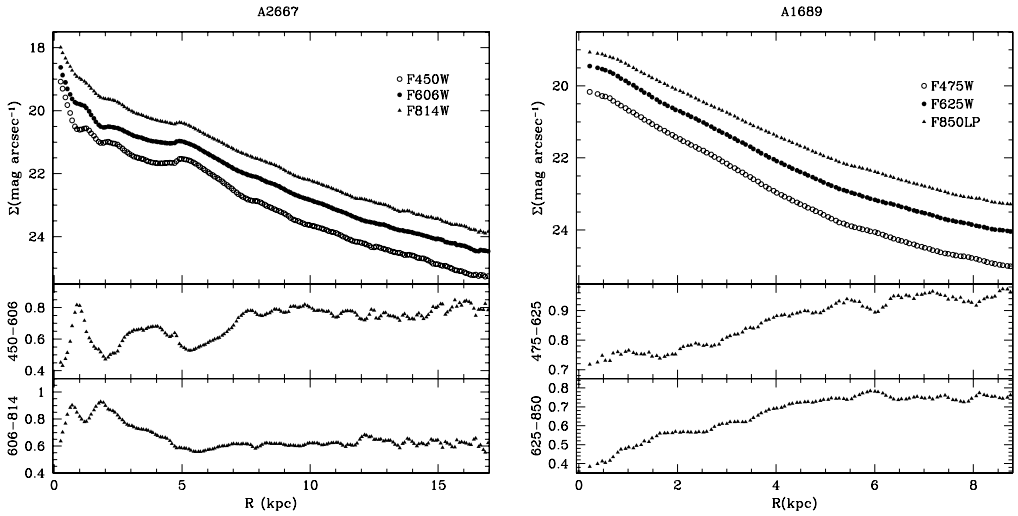

Figure 4. The surface brightness and colour profiles in the three *HST* bands for 235144−260358 in Abell 2667 (left) 131124−012040 in Abell 1689 (right).

is dominated by a combination of the polycyclic aromatic hydrocarbon (PAH) bump (≈6.2 μm) and very small grains continuum (Desert, Boulanger & Puget 1990), while the old stellar population dominates at shorter wavelengths. The observed 8/5.6 μm flux ratio ≈6.3 (corresponding to the rest-frame flux ratio 6.3/4.5 μm) is consistent with the value observed in star-forming galaxies (Dale et al. 2005), suggesting that the infrared emission is due to recent star formation activity.

We used the X-ray data for a second test of whether the infrared emission is due to a burst of star formation or to an active galactic nucleus (AGN). Comparing the X-ray upper limit to the 24-μm flux density (see Table 1) with the help of fig. 1 of Alonso-Herrero et al. (2004) confirms that this source is not AGN dominated: its 2–10 keV/24 μm flux ratio is at least four times too low to lie within the range of typical AGN.[3] Finally, a significant contribution from an AGN is ruled out by the emission-line ratios obtained from the optical spectrum: $\log([\mathrm{O\,III}]/\mathrm{H}\beta) \approx -0.45$, $\log([\mathrm{N\,II}]/\mathrm{H}\alpha) \approx -0.33$ consistent with the values typically observed in star-forming galaxies (Kewley et al. 2001). We therefore used the 8- and 24-μm data to derive the total infrared luminosity, L(IR), using the IR spectral energy distribution (SED) from the Chary & Elbaz (2001) and Dale & Helou (2002) library following the procedure described in Marcillac et al. (2006). This method relies on the correlations between L(IR) versus the luminosity at 7 μm and L(IR) versus L(24 μm) shown in Chary & Elbaz (2001). The SED templates were only used to interpolate at 8 and 24 μm. The resulting total infrared luminosity of 235144−260358 $L(\mathrm{IR}) \approx 3(\pm 0.25) \times 10^{11}\,\mathrm{L}_{\odot}$, implies a current star formation rate (SFR) $\approx 53(\pm 4.3)\,\mathrm{M}_{\odot}\,\mathrm{yr}^{-1}$ (using the relation of Kennicutt 1998), consistent with a SFR $\approx 57\,\mathrm{M}_{\odot}\,\mathrm{yr}^{-1}$ obtained from VLA continuum observations and the relation of Condon (1992). This galaxy is a rare example of a luminous infrared galaxy (LIRG) in a dense cluster.

All the properties of 235144−260358 point out the peculiarity of its recent evolutionary history. However, the extended trails of bright blue knots, tracing its trajectory as it falls into the cluster

[3] Neither of these tests can exclude the presence of a Compton thick AGN (Shi et al. 2005), but it is likely that the mid-infrared output of such objects is dominated by star formation.

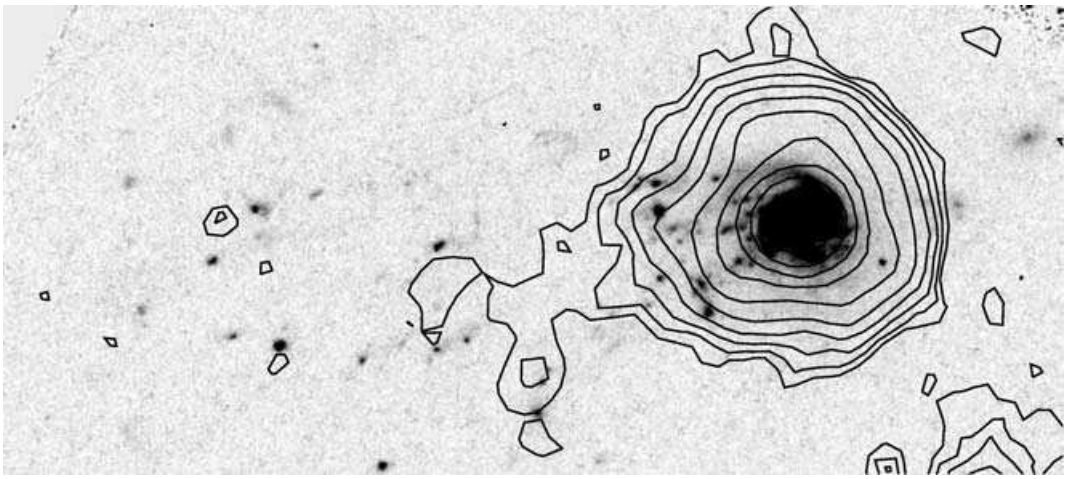

Figure 5. *HST* F450W image of 235144−260358 in Abell 2667. The Spitzer 8-μm contours are superposed in black. The lower contour corresponds to a 3σ noise level ($\approx$0.23 μJ arcsec^{-2}).

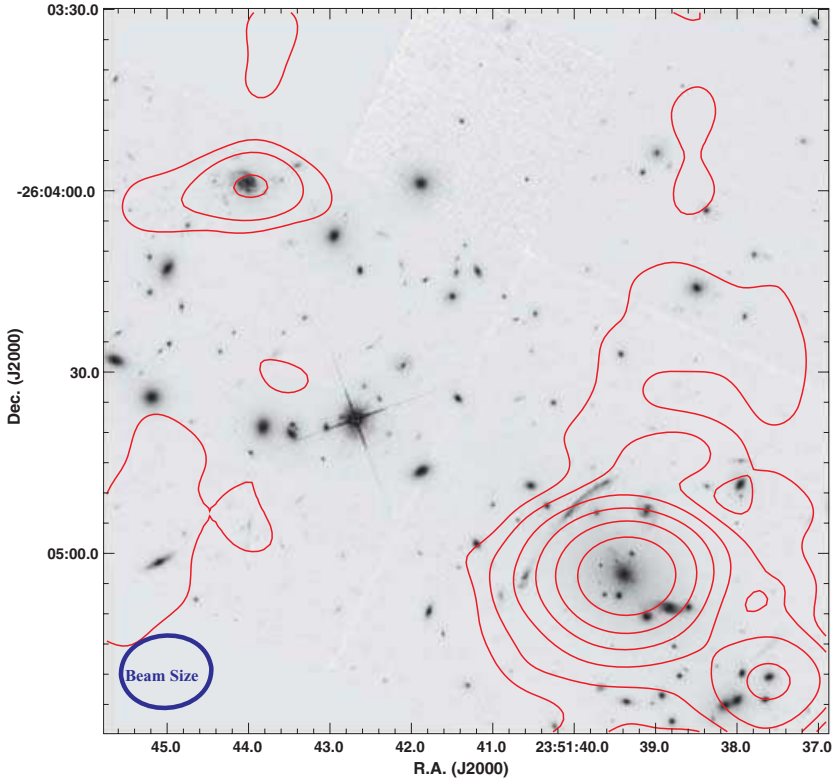

Figure 6. The VLA 20-cm radio contours (2σ, 4σ, 8σ, 16σ, 34σ and 64σ) of Abell 2667 superposed on the *HST* F450W image.

core, make it truly extraordinary. A dozen such knots extend from the galaxy optical disc to a projected distance of $\approx 80\,h_{70}^{-1}$ kpc. Extended blue low surface brightness wisps and filaments lie along the same trail, supporting the hypothesis that all of these structures result from stripping (see Fig. 3). The knots have absolute F450W magnitudes in the range $-16.80 < M_{\rm F450W} < -14.80$ mag, typical of dwarf galaxies (Sandage, Binggeli & Tammann 1985) and super-star clusters (Larsen & Richtler 1999), and are barely resolved in the *HST* image implying an effective radius $r_{\rm e} \leqslant 0.45\,h_{70}^{-1}$ kpc.

The radio contours shown in Fig. 6 appear elongated in the direction of the trail. A similar morphology seems also to be present in the Spitzer 8-μm map shown in Fig. 5, which has the appearance of a head on the galaxy, with a tail tracing the current star formation associated with the blue knots. Moreover, [O II] emission, not associated with any of the blue knots, extends from the galaxy for a total length of at least $\approx$50 kpc (see Fig. 8), suggesting the presence of diffuse ionized gas along the trails as already observed in nearby ram pressure stripped galaxies (Gavazzi et al. 2001; Yoshida et al. 2004; Cortese et al. 2006b).

To constrain the ages of the blue knots, we compute the time evolution of the F450W−F606W and F606W−F814LP colours, using STARBURST99 (Leitherer et al. 1999). We assume a Salpeter initial

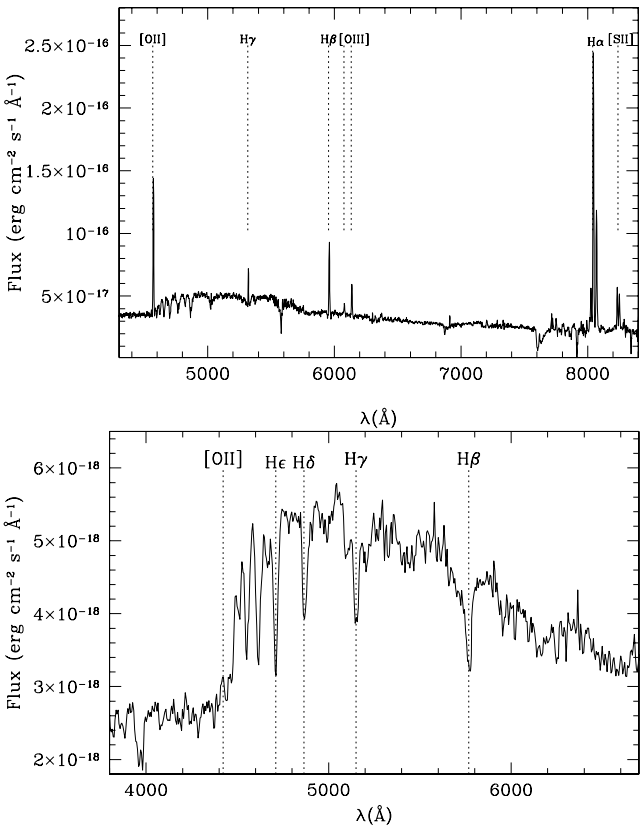

Figure 7. The optical spectrum of 235144−260358 in Abell 2667 (upper) and 131124−012040 in Abell 1689 (lower). The main emission and absorption lines are indicated.

mass function (IMF), solar metallicity[4] and two different star formation histories: an instantaneous burst and continuous star formation. For each star formation history we also compute a model including the contribution of strong emission lines. We redshifted the synthetic Starburst99 spectra to the cluster distance and used the synthetic photometry package SYNPHOT in IRAF to compute the model colours in the WFPC2 pass bands. In Fig. 9, we plot a colour–colour diagram for the bright knots (black circles) to compare with the theoretical evolutionary tracks (solid and dashed lines). We present only the colours for the brightest knots, i.e. detected in all three *HST* bands (see Fig. 3). The arrow shows the effect of attenuation by dust on the observed colours, assuming a Galactic attenuation curve (Schlegel, Finkbeiner & Davis 1998). The models with emission lines (dashed lines) appear to fit the observed colours better than those without (solid lines). Most of the blue knots lie slightly below the modelled tracks for both an instantaneous burst and continuous star formation but are reasonably consistent with an age of the episode in the range $5 < t < 15$ Myr in the first case and $10 < t < 1000$ Myr in the second case. These values are probably upper limits since it is very likely that the star-forming knots contain dust, as observed in extragalactic H II regions (Gerhard et al. 2002; Cortese et al. 2004) and star-forming dwarf galaxies (Boselli, Gavazzi & Sanvito 2003; Cortese et al. 2006a).

[4] We also tested a Kroupa IMF and stellar metallicities in the range $0.004 < Z < 0.02$, but the evolutionary paths do not significantly vary from the ones shown in Fig. 9.

Our spectra detect [O II] in emission in both the knots (K1 and K2) included on the slit (see Fig. 8) confirming that these systems are still forming stars. For K1 we also detected [O III] and Hα in emission ($z \approx 0.227$). The Hα flux is $f \approx 1.6 \times 10^{-17}$ erg cm^{-2} s^{-1} corresponding to a SFR ≈ 0.02 M$_\odot$ yr^{-1} (not corrected for extinction). No continuum is detected above a flux limit $f \approx 3 \times 10^{-19}$ erg cm^{-2} s^{-1} A^{-1}, implying an Hα equivalent width EW(Hα) $\geqslant 50$ Å. The lower limit on EW(H α) corresponds to an age of the knots $t \leqslant 5$ Myr for an instantaneous burst (Leitherer et al. 1999). This value is significantly shorter than the one obtained from the optical colours (see Fig. 9) implying a significant larger amount of dust in the knots ($A_V \approx 0.5$–1 mag) than the one observed in their parent galaxy ($A_V \approx 0.31$ mag). In comparison, for a continuous star formation history the value of EW(Hα) corresponds to an age $t \leqslant 1000$ Myr, consistent with the estimate obtained from the optical colours, making this scenario much more likely.

3.2 Abell 1689

The disrupted galaxy in Abell 1689 is illustrated in Fig. 3 (lower panel) and its main properties are listed in Table 1. This galaxy lies at a projected distance $\approx 0.24\, h_{70}^{-1}$ Mpc from the cluster centre (see Fig. 2) and is ≈2.5 mag fainter than the perturbed galaxy in Abell 2667 (i.e. with a luminosity of $\approx 0.1 L^*$; Wilson et al. 1997). Its redshift is $z \approx 0.1866$ confirming that it belongs to A1689. Contrary to 235144−260358, the surface brightness profile of this galaxy follows a typical exponential profile (see Fig. 4). However, the slopes of its colour profiles are anomalous: in both F450W − F625W and F625W − F814W there is an inversion of the colour gradients, with bluer colours toward the centre. The galaxy outskirts have a F450W − F814W colour ≈1.7 mag, ≈0.6 mag redder than the galaxy centre and consistent with the typical colour of red sequence galaxies in the local Universe (Bernardi et al. 2003). Similar features have been observed in spiral galaxies in the Virgo cluster and suggest recent ($t \leqslant 300$ Myr) gas stripping by ram pressure (Boselli et al. 2006). 131124−012040 is neither detected at 24 μm by Spitzer nor in VLA continuum images (see Table 1). This is consistent with the optical spectrum of this galaxy (see Fig. 7), which shows strong Balmer lines in absorption (EW (H δ) ≈ 6 Å, $D(4000) \approx 1.21$) and very little residual star formation (EW([O II]) ≈ 1.8 Å). This overall behaviour suggests that the galaxy centre has recently ($t \leqslant 100$ Myr; e.g. Poggianti & Barbaro 1997; Shioya et al. 2002; Kauffmann et al. 2003) stopped forming stars. These spectral features are consistent with both a simple truncated and a post-starburst SFH (Shioya et al. 2002; Pracy et al. 2005; Crowl & Kenney 2006), however, the inverted colour gradients and the absence of a central enhancement in the surface brightness profile favour a ram pressure scenario (Bekki et al. 2005; Boselli et al. 2006).

A $\approx 30\, h_{70}^{-1}$ kpc long trail, formed of at least six blue knots and a number of wisps and filaments, is associated with this system. The bright knots have absolute F475W magnitudes in the range $-13.5 < M_{\rm F475W} < -11.5$ mag, lying between dwarf galaxies and stellar clusters (≈3 mag fainter than the knots observed in Abell 2667).[5] The knots nearest to the galaxy are clearly resolved in the *HST* images and have a typical size $r_{\rm e}$(F475W) ≈ 0.8–0.9 kpc. In comparison, the most distant knots are not resolved implying a physical size $r_{\rm e}$(F475W) $\leqslant 0.35$ kpc. To determine the ages of the blue knots we

[5] ACS observation of A1689 are ≈3 mag deeper than WFPC2 imaging of A2667. We cannot, therefore, exclude that knots as faint as the one in A1689 are present also in A2667.

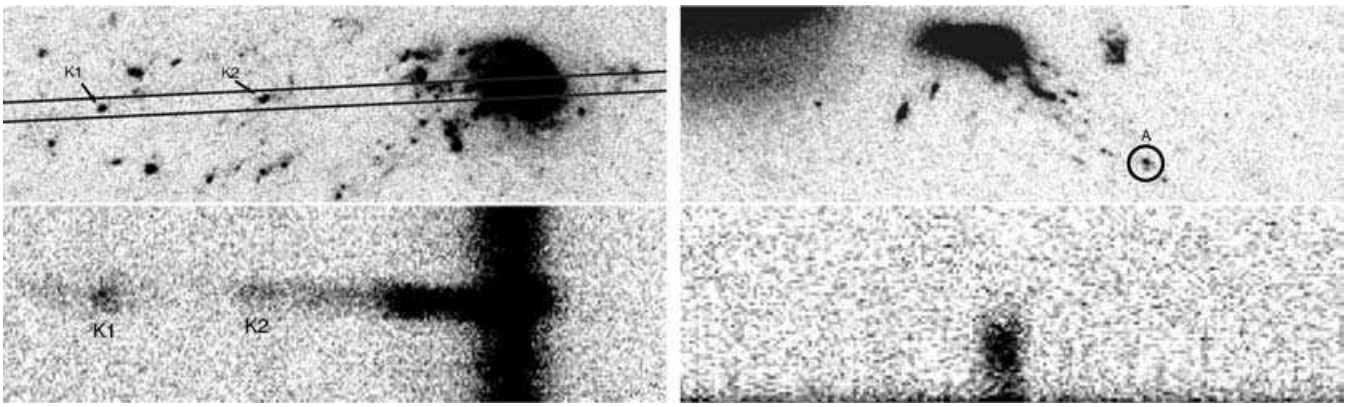

Figure 8. Left: the 2D spectrum of 234144−260358 in Abell 2667 and of two blue knots near the wavelength of the [O II] emission line (lower panel). The slit position is indicated by the two solid lines in the upper panel. [O II] diffuse emission appears clearly between the galaxy and the blue knots. Right: the 2D spectrum of knot A in Abell 1689 near the wavelength of the [O II] emission line (lower panel). The position of the knot is indicated by the black circle in the upper panel.

computed the time evolution of the F475W − F625W and F625W − F850LP colours, as described in the previous section. The results of our analysis are presented in Fig. 9. Most of the knots lie within the modelled tracks for an instantaneous burst with an age in the range $5 < t < 100$ Myr, and are slightly above the model for continuous star formation with an age in the range $10 < t < 1000$ Myr. As for 235144−260358 no correlation is observed between the optical colours of the knots and their distance from the infalling galaxy (see Fig. 10). The optical spectrum obtained for the most distant knot (Knot A in Fig. 8) reveals the presence of strong [O II] in emission ($f \approx 5.4 \times 10^{-17}$ erg cm^{-2} s^{-1} Å^{-1}), while no continuum is detected at a limit $\approx 5 \times 10^{-19}$ erg cm^{-2} s^{-1} Å^{-1}, implying an EW[O II] $\geqslant$ 108 Å and showing that star formation is still taking place in this system. Also Hα emission is detected, but it lies on a bright skyline and is affected by fringing making it impossible to use the Hα equivalent width to obtain an independent estimate of the age of the burst. It is interesting to note that the time-scale necessary to invert the colour gradients ($t \leqslant 300$ Myr) appears to be slightly longer than the age of the trails ($t < 100$ Myr), suggesting that the two features could be signatures of different physical mechanisms.

4 ENVIRONMENTAL EFFECTS ON THE EVOLUTION OF THE INFALLING GALAXIES

The peculiar properties of the two galaxies falling into A2667 and A1689 suggest that both galaxies are undergoing strong transformations due to their interaction with the harsh cluster environment. However, while these objects are at similar distances from the cluster centres and show similar extended trails of star-forming knots, their recent star formation histories are different. 235144−260358 is experiencing a strong burst of star formation, appearing as a rare example of a luminous infrared cluster galaxy. In comparison, 131124−012040 has recently ($t \leqslant 100$ Myr) ceased its star formation activity. To probe this difference, we investigate the effects of different environmental mechanisms on the properties and star formation history of these two galaxies.

The high velocity dispersion of the two clusters ($\sigma_{1D} \geqslant 1000$ km s^{-1}; Covone et al. 2006a; Łokas et al. 2006) makes very unlikely a low velocity interaction or a merger with another cluster galaxy. This would not be the case if the two galaxies belong to smaller, kinematically distinct, dynamical units (e.g. infalling groups). However, no observational evidences support this possibility. Therefore, we will only consider high velocity galaxy–galaxy and galaxy–cluster gravitational interactions and ram pressure stripping by the hot ICM as possible mechanisms to explain the peculiarities of these two galaxies.

In order to reduce the number of free parameters in our model we assume that the two galaxies are falling on linear orbits into the cluster core. This very simple scenario, supported by the fact that infalling galaxies have usually highly eccentric radial orbits (Boselli & Gavazzi 2006), allow us to express the cluster-centric distance (r) as a function of the galaxy infalling velocity:

$$r = \frac{r_{\rm proj}}{\sin(\arccos(V_{\rm ls}/V_{\rm infall}))}, \quad (1)$$

where $V_{\rm ls}$ is the (measured) velocity component along the line of sight and $r_{\rm proj}$ is the cluster-centric distance projected along the line of sight. Similarly, assuming that the trails of blue knots trace the galaxy's trajectory (Moore et al. 1999), their physical length is

$$L_{\rm trail} = \frac{L_{\rm proj}}{\sin(\arccos(V_{\rm ls}/V_{\rm infall}))}, \quad (2)$$

where $L_{\rm proj}$ is their projected length and their age is

$$t_{\rm trails} = \frac{L_{\rm trail}}{V_{\rm infall}}. \quad (3)$$

This value of $t_{\rm trails}$ is based on the assumption that the trails are at rest with respect to the cluster, and must be considered as a lower limit for the real age of these features.

Both clusters have a one-dimensional (1D) velocity dispersion $\sigma_{1D} \geqslant 1000$ km s^{-1} (Covone et al. 2006a; Łokas et al. 2006), implying a three-dimensional (3D) infalling velocity $V_{\rm infall} \approx \sqrt{3}\sigma_{1D}$. In the following we therefore assume a 3D infalling velocity in the range $1000 < V_{\rm infall} < 1730$ km s^{-1} (i.e. $\sqrt{3}\sigma_{1D}$ and σ_{1D}) that can be considered as upper and lower limit of the real value. The values so derived for the cluster-centric distance, the length and the age of the trails for the upper and lower limit of $V_{\rm infall}$ are summarized in Table 2.

4.1 Gravitational interactions

We can approximate the strengths of high velocity galaxy–galaxy and galaxy–cluster interactions by using the impulse approximation (Henriksen & Byrd 1996). The transverse and radial tidal

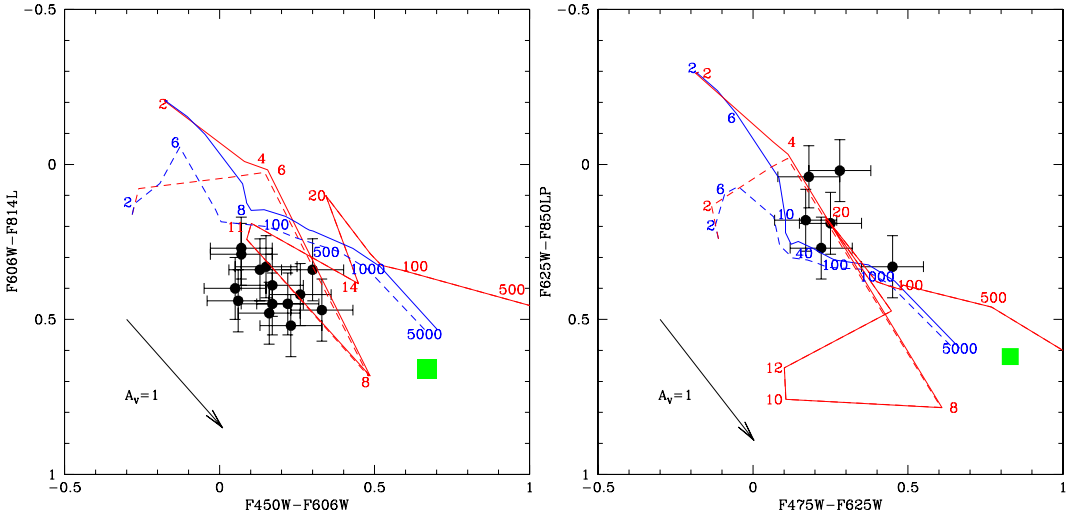

Figure 9. Colour–colour diagram for the blue knots in Abell 2667 (left) and Abell 1689 (right). The black circles with their associated error bars represent the knot colours and their uncertainties. The green squares indicate the colours of the two disrupted galaxies. The dashed lines are the model predictions for the evolution of simple stellar populations (SSPs) (red) and continuous (blue) star formation accounting for the contribution of emission lines. The solid lines represent the same models without the contribution of emission lines. The numbers indicate the age of each model in Myr. The black arrows show the effect of internal extinction on the observed colours. This figure is in colour in the online version of the article on *Synergy*.

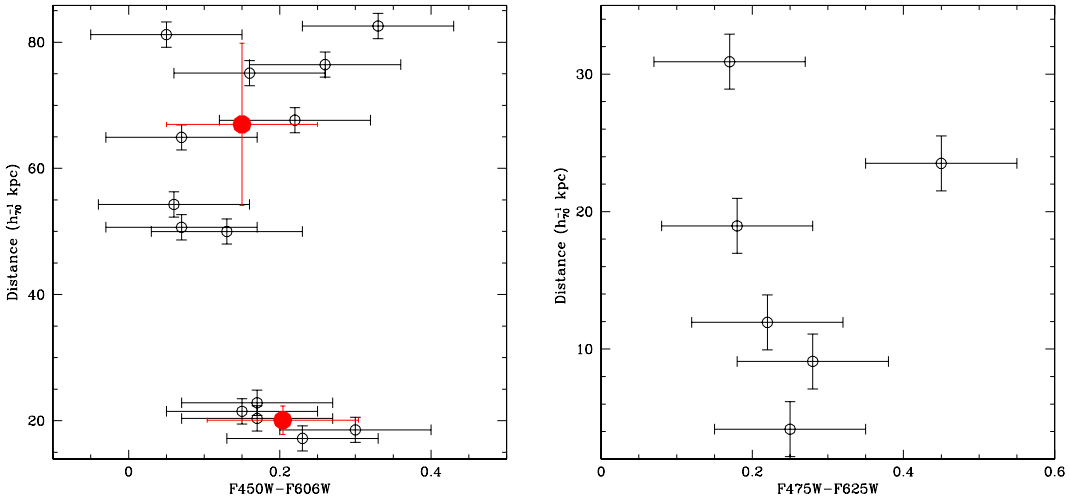

Figure 10. Left: distribution of the F450W − F606W colours for the star-forming knots in Abell 2667 as a function of the distance from 235144−260358. The red points represent the average values for the nearest and most distant star-forming knots. Right: the same diagram for the F475W − F650W colour of the star-forming knots associated with 131124−012040 in Abell 1689. This figure is in colour in the online version of the article on *Synergy*.

Table 2. Cluster centric distances and properties of the trails as a function of the 3D infalling velocity assumed in the model described in Section 4.

Cluster	$V_{\rm infall} \approx 1730\,{\rm km\,s^{-1}}$			$V_{\rm infall} \approx 1000\,{\rm km\,s^{-1}}$		
	D kpc	$L_{\rm trails}$ kpc	$t_{\rm trails}$ Myr	D kpc	$L_{\rm trails}$ kpc	$t_{\rm trails}$ Myr
A1689	280	35	20	450	60	60
A2667	390	90	54	610	140	150

accelerations experienced by the infalling galaxy are

$$a_{\rm tr} = GM_{\rm pert}\frac{R}{[R^2+(r+R)^2]^{1.5}}, \quad (4)$$

$$a_{\rm rad} = GM_{\rm pert}\left[\frac{1}{r^2}-\frac{1}{(r+R)^2}\right], \quad (5)$$

where $M_{\rm pert}$ is the mass of the perturber within r, R is the radius of the perturbed galaxy (assumed to be ≈5 effective radii; Gavazzi et al. 2000) and r is its distance from the perturber. The radial tidal field tends to accelerate the edge of a galaxy. If it is more intense than the internal galaxy acceleration, given by

$$a_{\rm gal} = \frac{GM_{\rm dyn}}{R^2}, \quad (6)$$

where $M_{\rm dyn}$ is the dynamical galaxy mass, it is able to strip material from the infalling galaxy. Following Gavazzi, Pierini & Boselli (1996), we use the H-band rest-frame luminosity of the two galaxies to estimate their dynamical masses within the optical radius and derive their disc rotational velocities obtaining $M_{\rm dyn} \approx 10^{11.6}$ and $10^{10.6}\,{\rm M}_{\odot}$ for 235144−260358 and 131124−012040, respectively. In the case of non-interpenetrating galaxy–galaxy interactions, the impact parameter is at least equal or greater than the galactic

radius (i.e. $r \geqslant R$) implying that material is stripped from an infalling galaxy only if

$$M_{\rm pert} \geqslant 1.33\, M_{\rm dyn} \tag{7}$$

(i.e. $\approx 10^{11.7}$ and $10^{10.7}\,{\rm M}_{\odot}$ for 235144−260358 and 131124−012040, respectively). The possible perturber should not lie at a larger distance than the typical size of trails. In Abell 2667, the brightest objects within a projected distance of 100 kpc from 235144−260358 have an H-band magnitude ≈ -24.5 mag (i.e. $M_{\rm dyn} \approx 10^{11.6}\,{\rm M}_{\odot}$), fairly consistent with the lower limit required for effective stripping. Unfortunately, their recessional velocities are unknown, making impossible a more detailed analysis of their possible interaction with 235144−260358. In Abell 1689, the giant face-on barred spiral projected at ≈20-kpc NE from 131124−012040 (see Fig. 2) is the only object (within 100 kpc) satisfying equation (7). However, the trail of blue knots is pointing in the opposite direction than the one expected in the case of interaction between the two objects (i.e. towards the perturber) and the galaxy has a redshift of $z \approx 0.1924$, i.e. 1680 km s^{-1} higher than the recessional velocity of 131124−012040, making unlikely an interaction between the two objects.

To quantify the effect of tidal forces from the cluster potential well on an infalling galaxy, we assume a NFW profile (Navarro, Frenk & White 1997) for the cluster mass distribution:

$$M(<r) = M_0 \left[\ln\left(1 + \frac{r}{r_{\rm s}}\right) - \frac{r/r_{\rm s}}{1 + r/r_{\rm s}} \right] \quad \text{for } r \leqslant r_{\rm s} c, \tag{8}$$

where

$$M_0 = 4\pi \frac{3H_0^2}{8\pi G} \left[\Omega_M (1+z)^3 + \Omega_\Lambda\right] \frac{200 c^3 r_{\rm s}^3}{3[\ln(1+c) - c/(1+c)]} \tag{9}$$

and $r_{\rm s}$ and c are the scale radius and concentration parameter of the mass distribution. The values adopted for the two clusters are summarized in Table 3. As shown in Fig. 11, for both our galaxies the radial acceleration from the cluster potential is higher than the internal acceleration for a cluster-centric distance smaller than $\approx 0.45\, h_{70}^{-1}$ Mpc. Therefore, depending on their real infalling velocity, the two objects are at the edge or are just entered the region where material can be efficiently stripped by gravitational interactions. This simple calculation gives a lower limit for the real efficiency of mass loss, since higher rates will occur in the presence of substructures and infalling groups, as is likely in these two clusters (Covone et al. 2006b; Łokas et al. 2006). Moreover, tidal heating (Taylor & Babul 2001) produced by the varying cluster gravitational field will significantly accelerate mass loss (Gnedin 2003b,a), although it is not considered in our model.

In contrast to the radial acceleration, which tends to strip material from an infalling galaxy, the transverse field compresses the interstellar medium to produce gas infall toward the centre and may trigger a burst of star formation. Gas clouds experience a velocity perturbation due to the transversal tidal acceleration and collide with other gas clouds. The increase in the cloud velocity can be estimated as

$$V = \int a_{\rm tr}\, {\rm d}t \approx a_{\rm tr} \Delta(t), \tag{10}$$

where $\Delta(t)$ is the age of the interaction. The velocity increase and cloud collision produce a density enhancement in the centre of the galaxy, which is proportional to the Mach number (MN) squared. Consequently the critical mass for the cloud collapse (which is proportional to $\rho_{\rm gas}^{-0.5}$) decreases by a factor MN^{-1} and, in the case of a strong perturbation, could become smaller than the typical mass of a galactic disc H I cloud (≈300 M$_{\odot}$; Spitzer 1978; Jog & Solomon 1992), favouring new episodes of star formation (Henriksen & Byrd 1996). Fig. 12 shows the ratio between the typical mass of H I clouds and the critical mass for cloud collapse in the case of high velocity interactions, assuming $M_{\rm pert} \approx 10^{11.6}$ and $10^{11.3}\,{\rm M}_{\odot}$ for 235144−260358 and 131124−012040, respectively, as discussed above. It appears that in both cases high velocity galaxy–galaxy interactions are not enough strong to trigger a burst of star formation as observed in 235144−260358.

This is not the case of galaxy–cluster interactions. Fig. 13 shows again the ratio between the typical mass of H I clouds and the critical mass for cloud collapse as a function of the cluster-centric distance in case of interaction with the cluster potential. In this case two galaxies are in two different regimes, whatever are the initial conditions in our model. While in 235144−260358 the critical mass is already below ≈300 M$_{\odot}$ and the compressed gas is able to collapse and produce new stars, in 131124−012040 this is still not the case. This result is consistent with our observations and indicates that tidal forces from A2667 may have triggered the strong starburst in 235144−260358.

In summary our model suggests that gravitational interactions with the cluster potential alone are able to strip material from the two infalling galaxies and to trigger a burst of star formation in

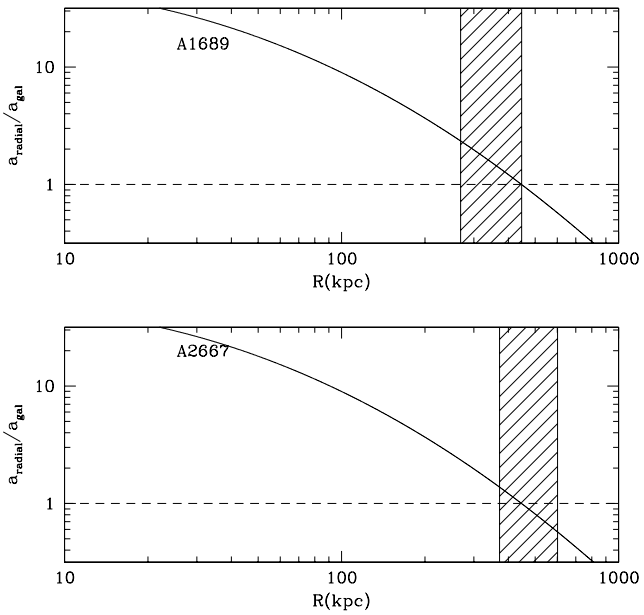

Figure 11. The ratio of the radial acceleration due to the cluster potential to the internal galaxy acceleration as a function of the cluster-centric distance for A1689 (upper panel) and A2667 (lower panel). The shaded regions indicate the range of cluster-centric distances assumed in the model (see Section 4).

Table 3. Best-fitting parameters for the total mass and gas density profiles of A1689 and A2667.

Cluster	Mass profile			Gas profile			
	$r_{\rm s}$ Mpc	c	Ref.	β	$R_{\rm c}$ Mpc	ρ_0 g cm^{-3}	Ref.
A1689	0.31	8.2	1	0.55	0.07	1.77×10^{-24}	3
A2667	0.49	6	2	0.52	0.049	2.17×10^{-24}	3

References: 1 – Broadhurst et al. (2005); 2 – Covone et al. (2006a); 3 – Ota & Mitsuda (2004).

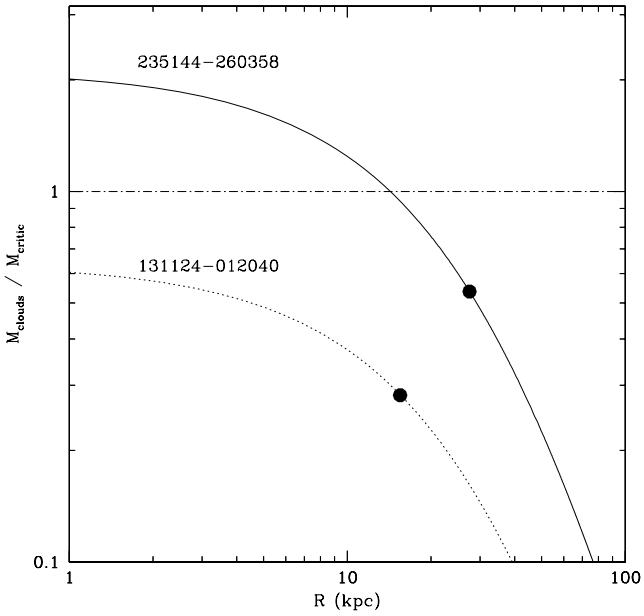

Figure 12. The ratio of the typical H I cloud mass in galactic discs to the critical mass for gas collapse in the case of galaxy–galaxy interactions as a function of the distance from the perturber for 235144−260358 in Abell 2667 (solid line) and of 131124−012040 in Abell 1689 (dotted line). The black circles indicate the values for the closest interaction possible ($r \approx R_{\rm gal}$). The horizontal dotted–dashed line shows the transition between the stable ($M_{\rm clouds}/M_{\rm critic} < 1$) and unstable ($M_{\rm clouds}/M_{\rm critic} > 1$) regime.

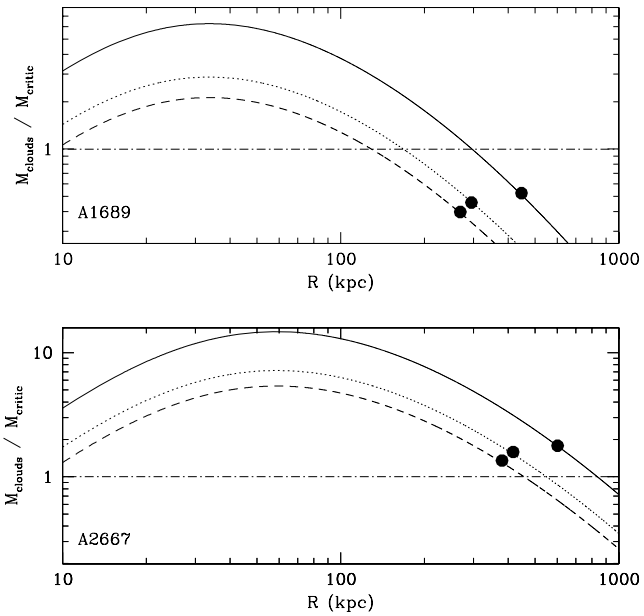

Figure 13. Same as Fig. 12 in case of a cluster–galaxy interaction in A1689 (upper panel) and A2667 (lower panel) for three different values of the 3D infalling velocity: 1000 km s^{-1} (solid line), 1410 km s^{-1} (dotted line) and 1730 km s^{-1} (dashed line). The black circles indicate the current galaxies positions assumed in each model.

235144−260358. Even if we cannot completely exclude a role of high velocity galaxy–galaxy interactions on the evolution of these systems, it appears clear that they cannot account for all the properties of the two infalling galaxies.

4.2 Ram pressure stripping

Although the tidal interaction hypothesis is consistent with the presence of a strong starburst only in 235144−260358, it is not able to explain why 131124−012040 shows clear signs of a recent truncation of its star formation. Both A1689 and A2667 are X-ray bright clusters suggesting that the effects of the hot ICM could be significant. Therefore, to estimate the effects of ram pressure stripping on the infalling galaxies, we adopt the classical Gunn & Gott (1972) criterion:

$$P_{\rm ram} = \rho_{\rm ICM} v^2 \geqslant 2\pi G \Sigma_{\rm star} \Sigma_{\rm gas}, \quad (11)$$

where $\rho_{\rm ICM}$ is the density of the intracluster medium, $\Sigma_{\rm star}$ and $\Sigma_{\rm gas}$ are the galaxy stellar and gas density and v is the 3D infalling velocity of the galaxy (here assumed to be in the range $1000 < v < 1730$ km s^{-1} as discussed in the previous sections). We use a β model density profile for the ICM:

$$\rho(r) = \rho_0 \frac{1}{\left[1 + \left(r/r_{\rm c}^2\right)\right]^{3\beta/2}} \quad (12)$$

(the values adopted for the different clusters are listed in Table 3). We assume that the stellar and gas distributions of our galaxies are exponential, as confirmed by their structural parameters. The gas and stellar density profiles are (Domainko et al. 2006)

$$\Sigma_{\rm star,gas}(r) = \frac{M_{\rm star,gas}}{2\pi R_{0\,\rm star,gas}^2} \exp(-r/R_{0\,\rm star,gas}), \quad (13)$$

where R_0 is the scalelength of the exponential profile (i.e. 0.59 $r_{\rm e}$). Assuming a gas scalelength $R_{0\,\rm gas} \approx 1.8\, R_{0\,\rm star}$ (Cayatte et al. 1994), a $M_{\rm gas}/M_{\rm star}$ ratio ≈1, typically observed in late-type galaxies (Boselli et al. 2001), and a $M_{\rm star}/L_{\rm H}$ ratio ≈1 (Gavazzi et al. 1996; McGaugh et al. 2000) the typical stripping radius is given by the following relation:

$$R_{\rm strip} \approx 0.64 R_0 \ln\left[\frac{G(L_{\rm H}/{\rm L}_\odot)^2}{1.8^2 \rho_{\rm ICM} v^2 2\pi R_{0\rm star}^4}\right], \quad (14)$$

and the mass of gas stripped by ram pressure is

$$M_{\rm strip} = \frac{L_{\rm H}}{{\rm L}_\odot}\left(\frac{R_{\rm strip}}{R_0} + 1\right)\exp(-R_{\rm strip}/R_0). \quad (15)$$

In Fig. 14 (left) we show the variation of the stripping radius as a function of the distance from the cluster centre for three different values of the 3D infalling velocities assumed in our model (≈1000, 1410 and 1730 km s^{-1}). While at its current location 131124−012040 has almost been totally stripped by ram pressure ($R_{\rm strip} \leqslant 0.9 r_{\rm e}$), in 235144−260358 ram pressure has only affected the outer galaxy regions ($R_{\rm strip} \geqslant 1.2 r_{\rm e}$). The same result can be analysed in terms of H I deficiency[6] (see Fig. 14, right). 131124−012040 has already lost ⩾80 per cent of its original gas content and if observed in a local cluster it would be classified as a highly H I-deficient object. Conversely, ram pressure has only stripped a tiny fraction of the gas from 235144−260358, whose H I deficiency (≈0.25) would approximately lie at the edge between normal and deficient galaxies (H I deficiency ≈ 0.2). We remark that the H I deficiency shown in

[6] The H I deficiency is defined as the difference, in logarithmic units, between the observed H I mass and the value expected from an isolated galaxy with the same morphological type T and optical linear diameter D: H I Def. = $\langle \log M_{\rm HI}(T^{\rm obs}, D_{\rm opt}^{\rm obs}) > - \log M_{\rm H\,I}^{\rm obs} \rangle$ (Haynes & Giovanelli 1984).

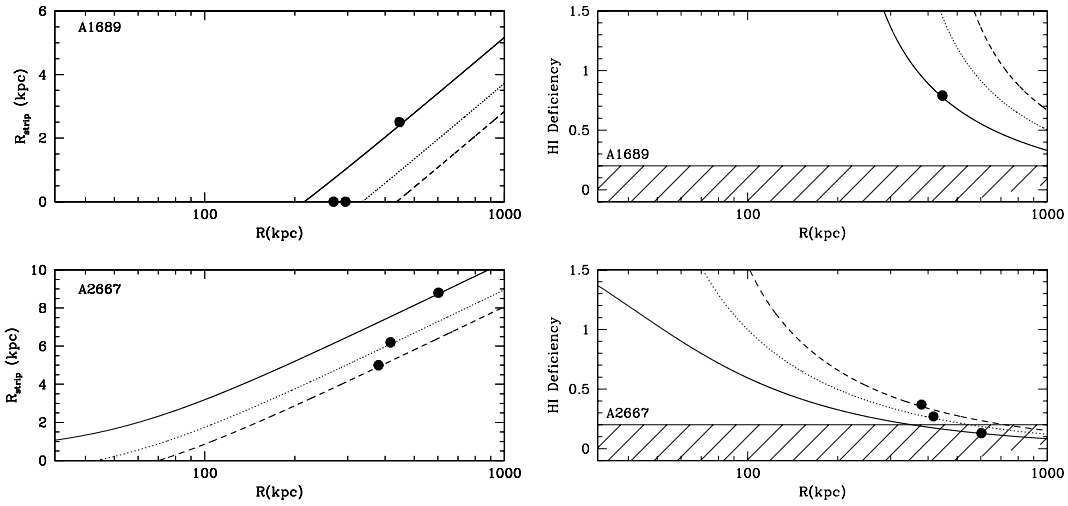

Figure 14. Left: the variation of the stripped radius as a function of the cluster-centric distance for 235144−260358 in Abell 2667 (lower panel) and of 131124−012040 in Abell 1689 (upper panel) for three different values of the 3D infalling velocity. Symbols are as in Fig. 13. Right: the variation of the H I deficiency as a function of the cluster-centric distance for 235144−260358 in Abell 2667 (lower panel) and of 131124−012040 in Abell 1689 (upper panel) for three different values of the 3D infalling velocity. The shaded area indicates the typical range of H I deficiency observed in unperturbed galaxies. Symbols are as in Fig. 13. For $V_{\rm infall} \geqslant 1200\,{\rm km\,s^{-1}}$ the galaxy has lost all its original H I content.

Fig. 14 is not determined from observations, but is obtained from our analytical model.

Comparing Fig. 14 to Fig. 11 it appears clear that ram pressure in 131124−012040 has become efficient before gravitational interactions were able to strip material from the galaxy. This is qualitatively consistent with the different time-scales of the interaction determined from the inversion of the colour gradients ($t \leqslant 300$ Myr, likely produced by ram pressure stripping) and from the blue star-forming trails ($t < 100$ Myr, clear signature of gravitational interactions).

4.3 The origin of the blue star-forming knots

The mutual effects of gravitational interactions and ram pressure have already been observed in several cluster galaxies, however, the tails of blue star-forming knots here discovered represent an extremely rare feature, to our knowledge previously observed only one other starburst galaxy in the Abell 2125 ($z \approx 0.247$; Owen et al. 2006). The morphology and luminosity of the knots suggest that we are dealing with dwarf galaxies and/or stellar superclusters (Fellhauer & Kroupa 2002). This could explain the observed difference between luminosity of the knots (≈2.5 mag) in the two galaxies since the luminosity of the brightest star clusters is usually correlated with the SFR of the parent galaxy (Weidner, Kroupa & Larsen 2004). The properties of the knots (i.e. colours and emission lines) suggest that they are undergoing an extended period of star formation as discussed in Section 3. From the model described in the previous sections the dynamical age of the trails results $50 < t_{\rm trail} < 150$ Myr and $20 < t_{\rm trail} < 60$ Myr for 235144−260358 and 131124−012040, respectively, fairly consistent[7] with the age inferred from their optical colours (see Fig. 9). It is impossible to determine whether the knots where already forming stars when they have been stripped or if their activity was triggered by an external mechanism once in the ICM. We can exclude that these systems have been formed in the ICM by the accretion of unbounded material stripped by the parent galaxies: the combined effects of the cluster tidal field and ram pressure tend to inhibit the formation of bound systems from the collapse of stripped material (Mihos 2004). This scenario is consistent with the numerical simulations. Elmegreen, Kaufman & Thomasson (1993) showed that gravitational interactions can lead to the formation and ejection of peripheral self-gravitationally bound clouds with masses $\leqslant 10^8$ M$_\odot$, which begin their life in a major burst of star formation. Moreover, Bekki & Couch (2003) have recently demonstrated that ram pressure can trigger the collapse of stripped clouds leading to a burst of star formation, suggesting that even the formation and evolution of the blue star-forming knots is probably driven by the mutual effects of gravitational interactions and ram pressure. Only deeper spectroscopic observations will shed light on the star formation history of these rare objects.

[7] However, the value of $t_{\rm trail}$ obtained in the previous section must be considered as a lower limit since it assumes that the stripped material is at rest with regard to the cluster.

5 DISCUSSION AND CONCLUSION

The analysis in this paper allows us to propose a scenario for the evolution of the two disturbed galaxies in Abell 2667 and 1689. These objects are currently falling into massive, gas-rich galaxy clusters with similar mass and gas density profiles (see Table 3). Under the combined action of tidal forces (more likely from the cluster potential) and of ram pressure by the ICM, their morphologies and star formation are strongly perturbed. Self-gravitational bound systems are ejected from the main galaxies and stars and ionized gas are stripped from the stellar discs producing the observed tails of blue knots and stellar wisps tracing the infalling trajectory of these systems into the cluster core. Only the tidal field of Abell 2667 is able to drive a gas infall into the centre of 235144−260358 triggering a nuclear burst of star formation and making this galaxy a rare example of luminous infrared cluster galaxy. Simultaneously ram pressure stripping by the hot ICM strips the neutral hydrogen from the galaxy outskirts but it is not able to affect the central regions where the starburst is taking place. Conversely in 131124−012040 gravitational forces are not strong enough to trigger the collapse

of gas clouds while ram pressure is already extremely efficient. At the present galaxy location ram pressure has stripped at least the ≈80 per cent of the original neutral hydrogen content, quenching the star formation activity in this object, as confirmed by the strong Balmer line in absorption observed in the optical spectrum (Shioya et al. 2002) and by the inversion of the optical colour gradients along all the galaxy extent (Boselli & Gavazzi 2006; Boselli et al. 2006).

A larger statistical sample is necessary to determine whether we are witnessing a common snapshot in the evolution of cluster galaxies or an extremely rare phenomenon. In fact, as discussed in the Introduction, only these two galaxies out of 13 different clusters imaged at $0.175 < z < 0.25$ show extended trails of blue knots. Within the WFPC2 field of view (≈0.25 Mpc^2 at $z \approx 0.2$) there are typically ≈50 cluster members but only the ≈20 per cent of them are spiral galaxies (Balogh et al. 2002), implying a frequency of ≈1.5 per cent (two over 130) among cluster spirals at $z \approx 0.2$. This value is fairly consistent with the expected frequency roughly obtained dividing the typical time-scale of the interaction ($\leqslant$200 Myr) to the age of the cluster (≈11 Gyr).

If we are witnessing a common step of cluster galaxy evolution what can we learn by studying these two rare objects? Abell 2667 and 1689 have comparable mass and gas profiles and the two galaxies are approximately at the same projected cluster-centric distance, suggesting that the absolute intensity of the cluster tidal field and of ram pressure by the cluster ICM is approximately the same in the two environments. Therefore, we can speculate that the different recent evolutionary history of the infalling systems could be in part related to their different properties (i.e. their different luminosities: $\approx L^*$ and $\approx 0.1L^*$). In this case, our result suggests that giant spiral galaxies infalling into the core of massive clusters are mainly perturbed by the gravitational interaction with the cluster. Stars respond by forming arms and bars, while the gas flows directly toward the central region within $t \approx 100$ Myr. The sinking of the gas towards the centre triggers a burst of star formation and is able to alter the galaxy morphology (Iono, Yun & Mihos 2004). Ram pressure stripping produces a truncation of the disc but only in the outskirts of the galaxy being not efficient within the optical effective radius. When all the remaining fuel has been consumed by the star formation this galaxy will no longer appear as a discy gas-rich systems but more likely as a bulge-dominated quiescent spiral. This is not the case for less massive galaxies. Ram pressure is much more efficient on low-mass systems and it is able to strip a considerable fraction of the neutral hydrogen from the inner part of these galaxies, preventing the gas from sinking toward the centre driven by tidal interaction and quenching the star formation history. Within ≈1 Gyr this object will not appear as a blue spiral any more but will probably look like an early-type (e.g. red) discy spiral (Shioya et al. 2002). The different evolutionary scenarios for the evolution of low and high mass infalling galaxies emerging from our analysis apparently fit with recent observations and models, suggesting that the bulk of the cluster population of giant bulge-dominated early-type spiral galaxies can only be formed during some kind of gravitational interaction (Dressler 2004; Mihos 2004), while lower mass systems can be transformed by simple gas removal from healthy spirals (Poggianti et al. 2004).

The properties of the blue knots stripped from the infalling galaxies deserve particular attention. These systems have a luminosity ($-16.5 \leqslant M \leqslant -11.5$) and a physical size ($r_e \leqslant 0.45$ kpc) typical of dwarf galaxies and consistent with the ultracompact dwarf (UCD) galaxies (Hilker, Infante & Richtler 1999; Phillipps et al. 2001), recently discovered in Abell 1689 (Mieske et al. 2004, 2005). There are two competing formation scenarios to explain the origin of UCDs. Bekki et al. (2003) propose that they are the remnants of stripped dwarf galaxies. In this scenario a nucleated dwarf loses its envelope and a great part of its dark matter content due to tidal interaction with another object. In contrast, Fellhauer & Kroupa (2002) propose that UCDs could origin from the *amalgamation* of rich aggregates of young massive star clusters that can form during gravitational interactions between gas-rich galaxies. It appears clear that the knots discovered here strongly support the second scenario, suggesting that at least part of the population of ultracompact dwarfs originate from young massive star clusters: we are probably for the first time witnessing the dawn of the UCDs. This scenario is also consistent with the recent discovery of a massive extragalactic star cluster ($M \geqslant 10^6\,\mathrm{M}_\odot$, $t \approx 700$ Myr) lying at a projected distance of 17 kpc from the merger remnant NGC 3310 and likely formed during the merging event (Knapp et al. 2006).

Finally, the diffuse stellar streams and ionized gas observed along the trails suggest that the mechanisms acting here will significantly influence the properties of the intracluster light and contribute to the enrichment of the ICM. The results here obtained might be representative only of the clusters at $z \geqslant 0.2$ where the infalling rate is higher and galaxies have an higher gas content than the one observed in local clusters of galaxies.

ACKNOWLEDGMENTS

We thank the referee, D. Christlein, for his useful comments which helped us to improve and strengthen the paper. LC is supported by the UK Particle Physics and Astronomy Research Council. Parts of the data presented herein were obtained at the W.M. Keck Observatory, which is operated as a scientific partnership among the California Institute of Technology, the University of California and the National Aeronautics and Space Administration. The observatory was made possible by the generous financial support of the W.M. Keck Foundation. This work was partially supported by NASA contract 1255094, administered by JPL/Caltech. JR acknowledges support from Caltech.

REFERENCES

Alonso-Herrero A. et al., 2004, ApJS, 154, 155
Balogh M. L., Morris S. L., Yee H. K. C., Carlberg R. G., Ellingson E., 1999, ApJ, 527, 54
Balogh M., Bower R. G., Smail I., Ziegler B. L., Davies R. L., Gaztelu A., Fritz A., 2002, MNRAS, 337, 256
Bekki K., Couch W. J., 2003, ApJ, 596, L13
Bekki K., Couch W. J., Drinkwater M. J., Shioya Y., 2003, MNRAS, 344, 399
Bekki K., Couch W. J., Shioya Y., Vazdekis A., 2005, MNRAS, 359, 949
Bernardi M. et al., 2003, AJ, 125, 1817
Bertin E., Arnouts S., 1996, A&AS, 117, 393
Boselli A., Gavazzi G., 2006, PASP, 118, 517
Boselli A., Gavazzi G., Donas J., Scodeggio M., 2001, AJ, 121, 753
Boselli A., Gavazzi G., Sanvito G., 2003, A&A, 402, 37
Boselli A. et al., 2005, ApJ, 623, L13
Boselli A., Boissier S., Cortese L., Gil de Paz A., Seibert M., Madore B. F., Buat V., Martin D. C., 2006, ApJ, 651, 811
Brandt W. N. et al., 2001, AJ, 122, 2810
Bravo-Alfaro H., Cayatte V., van Gorkom J. H., Balkowski C., 2000, AJ, 119, 580
Broadhurst T. et al., 2005, ApJ, 621, 53
Butcher H., Oemler A., 1978, ApJ, 226, 559
Butcher H., Oemler A., 1984, ApJ, 285, 426

Byrd G., Valtonen M., 1990, ApJ, 350, 89
Cayatte V., van Gorkom J. H., Balkowski C., Kotanyi C., 1990, AJ, 100, 604
Cayatte V., Kotanyi C., Balkowski C., van Gorkom J. H., 1994, AJ, 107, 1003
Chary R., Elbaz D., 2001, ApJ, 556, 562
Christlein D., Zabludoff A. I., 2004, ApJ, 616, 192
Condon J. J., 1992, ARA&A, 30, 575
Cortese L., Gavazzi G., Boselli A., Iglesias-Paramo J., 2004, A&A, 416, 119
Cortese L. et al., 2006a, ApJ, 637, 242
Cortese L., Gavazzi G., Boselli A., Franzetti P., Kennicutt R. C., O'Neil K., Sakai S., 2006b, A&A, 453, 847
Couch W. J., Barger A. J., Smail I., Ellis R. S., Sharples R. M., 1998, ApJ, 497, 188
Covone G., Kneib J.-P., Soucail G., Richard J., Jullo E., Ebeling H., 2006a, A&A, 456, 409
Covone G., Adami C., Durret F., Kneib J. P., Lima Neto G. B., Slezak E., 2006b, A&A, 460, 381
Crowl H. H., Kenney J. D. P., 2006, ApJ, 649, L75
Czoske O., 2004, in Diaferio A., ed., IAU Colloq. 195, Outskirts of Galaxy Clusters: Intense Life in the Suburbs, p. 183
Dale D. A., Helou G., 2002, ApJ, 576, 159
Dale D. A. et al., 2005, ApJ, 633, 857
Desert F.-X., Boulanger F., Puget J. L., 1990, A&A, 237, 215
Domainko W. et al., 2006, A&A, 452, 795
Dressler A., 1980, ApJ, 236, 351
Dressler A., 2004, in Mulchaey J. S., Dressler A., Oemler A., eds, Clusters of Galaxies: Probes of Cosmological Structure and Galaxy Evolution. Cambridge Univ. Press, Cambridge, p. 206
Dressler A., Smail I., Poggianti B. M., Butcher H., Couch W. J., Ellis R. S., Oemler A. J., 1999, ApJS, 122, 51
Duc P.-A., Brinks E., Springel V., Pichardo B., Weilbacher P., Mirabel I. F., 2000, AJ, 120, 1238
Dutil Y., Roy J., 1999, ApJ, 516, 62
Egami E. et al., 2006, ApJ, 647, 922
Elmegreen B. G., Kaufman M., Thomasson M., 1993, ApJ, 412, 90
Fadda D., Elbaz D., Duc P.-A., Flores H., Franceschini A., Cesarsky C. J., Moorwood A. F. M., 2000, A&A, 361, 827
Fazio G. G. et al., 2004, ApJS, 154, 10
Fellhauer M., Kroupa P., 2002, MNRAS, 330, 642
Fujita Y., 2004, PASJ, 56, 29
Gavazzi G., Pierini D., Boselli A., 1996, A&A, 312, 397
Gavazzi G., Franzetti P., Scodeggio M., Boselli A., Pierini D., 2000, A&A, 361, 863
Gavazzi G., Boselli A., Mayer L., Iglesias-Paramo J., Vílchez J. M., Carrasco L., 2001, ApJ, 563, L23
Gavazzi G., Zaccardo A., Sanvito G., Boselli A., Bonfanti C., 2004, A&A, 417, 499
Gavazzi G., Boselli A., Cortese L., Arosio I., Gallazzi A., Pedotti P., Carrasco L., 2006, A&A, 446, 839
Gerhard O., Arnaboldi M., Freeman K. C., Okamura S., 2002, ApJ, 580, L121
Giovanelli R., Haynes M. P., 1985, ApJ, 292, 404
Gnedin O. Y., 2003a, ApJ, 582, 141
Gnedin O. Y., 2003b, ApJ, 589, 752
Gómez P. L. et al., 2003, ApJ, 584, 210
Gunn J. E., Gott J. R. I., 1972, ApJ, 176, 1
Haynes M. P., Giovanelli R., 1984, AJ, 89, 758
Henriksen M., Byrd G., 1996, ApJ, 459, 82
Hilker M., Infante L., Richtler T., 1999, A&AS, 138, 55
Hinz J. L., Rieke G. H., Caldwell N., 2003, AJ, 126, 2622
Horne K., 1986, PASP, 98, 609
Iglesias-Páramo J., Vílchez J. M., 2001, ApJ, 550, 204
Iono D., Yun M. S., Mihos J. C., 2004, ApJ, 616, 199
Jeltema T. E., Canizares C. R., Bautz M. W., Buote D. A., 2005, ApJ, 624, 606
Jog C. J., Solomon P. M., 1992, ApJ, 387, 152
Kauffmann G. et al., 2003, MNRAS, 341, 33
Kenney J. D. P., Rubin V. C., Planesas P., Young J. S., 1995, ApJ, 438, 135
Kennicutt R. C., 1998, ARA&A, 36, 189
Kewley L. J., Dopita M. A., 2002, ApJS, 142, 35
Kewley L. J., Dopita M. A., Sutherland R. S., Heisler C. A., Trevena J., 2001, ApJ, 556, 121
Knapp G. R. et al., 2006, AJ, 131, 859
Krist J., 1995, in Shaw R. A., Payne H. E., Hayes J. J. E., eds, ASP Conf. Ser., Vol. 77, Astronomical Data Analysis Software and Systems IV. Astron. Soc. Pac., San Francisco, p. 349
Larsen S. S., Richtler T., 1999, A&A, 345, 59
Larson R. B., Tinsley B. M., Caldwell C. N., 1980, ApJ, 237, 692
Leitherer C. et al., 1999, ApJS, 123, 3
Lequeux J., Peimbert M., Rayo J. F., Serrano A., Torres-Peimbert S., 1979, A&A, 80, 155
Lewis I. et al., 2002, MNRAS, 334, 673
Łokas E. L., Prada F., Wojtak R., Moles M., Gottlöber S., 2006, MNRAS, 366, L26
McGaugh S. S., 1991, ApJ, 380, 140
McGaugh S. S., Schombert J. M., Bothun G. D., de Blok W. J. G., 2000, ApJ, 533, L99
Marcillac D., Elbaz D., Chary R. R., Dickinson M., Galliano F., Morrison G., 2006, A&A, 451, 57
Merritt D., 1983, ApJ, 264, 24
Mieske S. et al., 2004, AJ, 128, 1529
Mieske S., Infante L., Hilker M., Hertling G., Blakeslee J. P., Benitez N., Ford H., Zekser K., 2005, A&A, 430, L25
Mihos J. C., 2004, in Mulchaey J. S., Dressler A., Oemler A., eds, Clusters of Galaxies: Probes of Cosmological Structure and Galaxy Evolution. Cambridge Univ. Press, Cambridge, p. 278
Moore B., Katz N., Lake G., Dressler A., Oemler A., 1996, Nat, 379, 613
Moore B., Ghigna S., Governato F., Lake G., Quinn T., Stadel J., Tozzi P., 1999, ApJ, 524, L19
Navarro J. F., Frenk C. S., White S. D. M., 1997, ApJ, 490, 493
Oemler A. J., Dressler A., Butcher H. R., 1997, ApJ, 474, 561
Oke J. B. et al., 1995, PASP, 107, 375
Osterbrock D. E., 1989, Astrophysics of Gaseous Nebulae and Active Galactic Nuclei. University Science Books, Mill Valley, CA
Ota N., Mitsuda K., 2004, A&A, 428, 757
Owen F. N., Keel W. C., Wang Q. D., Ledlow M. J., Morrison G. E., 2006, AJ, 131, 1974
Papovich C. et al., 2004, ApJS, 154, 70
Pei Y. C., 1992, ApJ, 395, 130
Phillipps S., Drinkwater M. J., Gregg M. D., Jones J. B., 2001, ApJ, 560, 201
Poggianti B. M., Barbaro G., 1997, A&A, 325, 1025
Poggianti B. M., Bridges T. J., Komiyama Y., Yagi M., Carter D., Mobasher B., Okamura S., Kashikawa N., 2004, ApJ, 601, 197
Pracy M. B., Couch W. J., Blake C., Bekki K., Harrison C., Colless M., Kuntschner H., de Propris R., 2005, MNRAS, 359, 1421
Richard J., Pelló R., Schaerer D., Le Borgne J.-F., Kneib J.-P., 2006, A&A, 456, 861
Rieke G. H. et al., 2004, ApJS, 154, 25
Sandage A., Binggeli B., Tammann G. A., 1985, AJ, 90, 1759
Schlegel D. J., Finkbeiner D. P., Davis M., 1998, ApJ, 500, 525
Scodeggio M. et al., 2005, PASP, 117, 1284
Shi Y. et al., 2005, Am. Astron. Soc. Meeting Abstr., 207, 140.11
Shioya Y., Bekki K., Couch W. J., De Propris R., 2002, ApJ, 565, 223
Smith G. P., Kneib J.-P., Smail I., Mazzota P., Ebeling H., Czoske O., 2005, MNRAS, 359, 417
Spitzer L., 1978, Physical Processes in the Interstellar Medium. Wiley-Interscience, New York
Stetson P. B., 1987, PASP, 99, 191
Sulentic J. W., Rosado M., Dultzin-Hacyan D., Verdes-Montenegro L., Trinchieri G., Xu C., Pietsch W., 2001, AJ, 122, 2993
Taylor J. E., Babul A., 2001, ApJ, 559, 716
Treu T., Ellis R. S., Kneib J.-P., Dressler A., Smail I., Czoske O., Oemler A., Natarajan P., 2003, ApJ, 591, 53
Valluri M., 1993, ApJ, 408, 57

van Zee L., Salzer J. J., Haynes M. P., O'Donoghue A. A., Balonek T. J., 1998, AJ, 116, 2805
Vollmer B., 2003, A&A, 398, 525
Vollmer B., Cayatte V., Balkowski C., Duschl W. J., 2001, ApJ, 561, 708
Vollmer B., Balkowski C., Cayatte V., van Driel W., Huchtmeier W., 2004, A&A, 419, 35
Weidner C., Kroupa P., Larsen S. S., 2004, MNRAS, 350, 1503
Whitmore B. C., Gilmore D. M., Jones C., 1993, ApJ, 407, 489
Wilson G., Smail I., Ellis R. S., Couch W. J., 1997, MNRAS, 284, 915
Yoshida M. et al., 2004, AJ, 127, 90
Zaritsky D., Kennicutt R. C., Huchra J. P., 1994, ApJ, 420, 87

This paper has been typeset from a TEX/LATEX file prepared by the author.